Sonar Waveform Design for Optimum Target Detection: The Impact of Object Burial State

Brandon Hamschin
Dept. of Electrical & Computer Engineering
University of Pittsburgh
Pittsburgh, Pennsylvania 15261
Email: bmh52@pitt.edu

Patrick Loughlin
Depts. of Bioengineering, and ECE,
University of Pittsburgh
Pittsburgh, Pennsylvania 15261
Email: loughlin@pitt.edu

***Abstract*— The design of transmit waveforms in sonar and radar that optimize the probability of detection of a known target is an area of active interest. Previous research has demonstrated the benefits of optimal transmit waveforms for enhanced target detection, versus the transmission of more conventional waveforms such as broadband LFM pulses. For maximum benefit, the scattering function or frequency response of the target to be detected must be known, along with the spectral or statistical properties of the environment. In this paper, we examine the impact of a mismatch between the expected frequency response of the target, for which the optimal transmit waveform was designed, and the actual frequency response of the target. In particular, we design the optimal sonar transmit waveform based on the free-field response of the target, and then examine the effects on detection performance of burial of the target in sediment. Simulations of the sonar backscatter from a steel sphere in the water column and at various stages of burial demonstrate that the impact of mismatch becomes increasingly detrimental as the target becomes increasingly buried. For fully buried targets, the impact is such that transmitting a simple broadband LFM pulse can yield improved detection relative to "optimal" waveform design wherein there is a mismatch between the expected (free-field) and actual (buried) frequency response of the target.**

I. Introduction

The design of transmit waveforms for RADAR and SONAR that enhance the probability of detection of an object of interest has a long history and is an area that continues to receive active interest (e.g., [1]–[5], [7]–[10]). In this paper, we consider the impact of transmitting waveforms for optimizing the detection of underwater objects, particularly elastic objects, wherein the free-field response is known, but the target may be buried. The transmit waveform is designed based on the free-field response, and detection performance for various stages of target burial are examined through simulation.

While various optimality criteria have been considered, a common theme in the design of transmit waveforms for optimizing target detection is that the solution is specified in terms of the magnitude spectrum (the power spectrum or energy density spectrum) of the transmit waveform. The basic result is to design the magnitude spectrum so that there is energy in frequency bands where the target response is large relative to the effects of all sources of interference.

In this paper, we consider an optimal waveform design proposed by Kay [4], [5], which we apply to the detection of elastic targets [6]. We design the optimal transmit waveform based on the free-field frequency response of the target, and then examine the effects of target burial on performance. As a target becomes buried in sediment, the resonances shift, and there is attenuation of higher frequencies. Accordingly, a waveform that is optimal for the detection of the free-field target becomes suboptimal, and we examine via simulation the degradation in detection performance, relative to transmission of a simple broadband LFM pulse.

II. Background: Optimal Signal Design

In this section we summarize the main results from Kay [4], [5] to obtain the optimal transmit spectrum. Let $s(t)$ denote the optimal transmit waveform, with Fourier transform

$$S(\omega) = \frac{1}{\sqrt{2\pi}} \int s(t) e^{-j\omega t} dt \tag{1}$$

It is also convenient to express the spectrum in terms of amplitude $B(\omega) \geq 0$ and phase $\psi(\omega)$,

$$S(\omega) = B(\omega) e^{j\psi(\omega)} \tag{2}$$

In [4], Kay treats the problem of designing a signal that is optimal for detecting a point target in clutter and reverberation. This development assumes a single transmitter and a single receiver. Fig. 1 shows a block diagram model of the received signal, $x(t)$, that is processed by the optimal Neyman-Pearson detector, $D(x)$.

Our aim is to obtain the optimal transmit magnitude spectrum, $B_{opt}(\omega)$, for the case of a single transmitter, single receiver, and a single elastic target. With reference to Fig. 1, let $h(t)$ and $n(t)$ be Gaussian random processes and $g(t)$ be a deterministic LTI model of the elastic target. The detector that maximizes the probability of detecting $g(t)$ for a fixed false alarm rate P_{FA} is given by [5]

$$D(X) = \frac{2\pi}{T} \left| \int \frac{S^*(\omega) G^*(\omega) X(\omega)}{2\pi P_h(\omega) B^2(\omega) + P_n(\omega)} d\omega \right|^2 \tag{3}$$

where T is the observation duration of the received signal $x(t)$ which has Fourier transform $X(\omega)$, $s(t)$ is the known transmit signal with Fourier transform $S(\omega)$, and $G(\omega)$ is the Fourier transform of $g(t)$ (i.e., the frequency response of the object to be detected). The null hypothesis H_0 is rejected –

978-1-4244-5222-4/10/$26.00 ©2010 IEEE

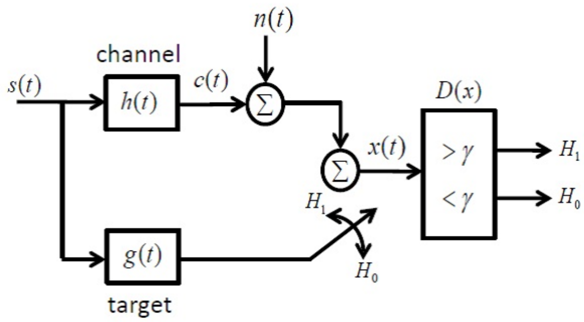

Fig. 1. Model of received signal $x(t)$, and associated detector $D(x)$. $s(t)$ is the transmitted signal; $h(t)$ is the impulse response of a random LTI filter that models channel interference induced by the transmit signal; $g(t)$ is the impulse response of the object to be detected; and $n(t)$ represents ambient noise.

i.e., a decision that the object is present is made – when $D(X)$ exceeds the threshold

$$\gamma = \sigma_0^2 \log(P_{FA}) \tag{4}$$

where

$$\sigma_0^2 = \frac{2\pi}{T} \int \frac{B^2(\omega)\,|G(\omega)|^2}{2\pi P_h(\omega) B^2(\omega) + P_n(\omega)} d\omega \tag{5}$$

Also, it can be shown the the performance of the detector in (3) is given by [4]

$$P_D = P_{FA}^{\frac{1}{1+\sigma_0^2}} \tag{6}$$

Finally, following the point target derivation in [4] we arrive at the magnitude squared spectrum of $s(t)$ that maximizes (6) for a fixed P_{FA}

$$B_{opt}^2(\omega) = \frac{1}{2\pi} \max\left(\frac{\lambda^{-1/2}\sqrt{\frac{2\pi}{T} P_n(\omega)\,|G(\omega)|^2} - P_n(\omega)}{P_h(\omega)}, 0 \right) \tag{7}$$

where λ is a constant, typically obtained numerically, that constrains the total energy of the transmit signal to some specified level, $\int B_{opt}^2(\omega) d\omega = E$.

In summary, if we are able to characterize the spectral properties of the target and the environment, we maximize the probability of detection by transmitting a signal whose magnitude spectrum is given by $B_{opt}(\omega)$. Often there is uncertainty or incomplete knowledge of the target and/or the environment. For example, in an ocean environment, objects of interest may be resting on the sea floor, or partially or completely covered by sediment. The effect of sediment on the frequency response of elastic objects has been previously explored and modeled in detail [13]–[17]. We use these results here to examine the impact of unknown burial state on the probability of detecting a specific object, given the free-field frequency response $G(\omega)$ of the object and the corresponding optimal transmit spectrum as obtained via Eq. (7).

	Water	Air	Steel	Sediment
Density	$1000\,\frac{kg}{m^3}$	$1.29\,\frac{kg}{m^3}$	$8000\,\frac{kg}{m^3}$	$2000\,\frac{kg}{m^3}$
Sound Speed	$1500\,\frac{m}{s}$	$344\,\frac{m}{s}$	$5688\,\frac{m}{s}$ (compressional) $3119\,\frac{m}{s}$ (shear)	1800 $-j7.5\,\frac{m}{s}$

TABLE I

PHYSICAL PARAMETERS

	Inner radius	Outer radius
Sphere	$0.2832\,m$	$0.2985\,m$

TABLE II

GEOMETRY OF SPHERICAL SHELL

III. SIMULATION RESULTS

Fig. 2 shows the six target burial states of a steel spherical shell that we consider in our simulations. We construct our simulations using the theoretical results and numerical codes which are based on the transition (T) matrix formalism found in [13]–[17]. The six target responses are given in Figs. 3 and 4. Also, the physical parameters of the top fluid (water), the sediment, the shell (steel), and its core (air) are summarized in Table I with the geometrical parameters of the spherical target given in Table II. The last main environmental factor that impacts the amount of acoustic energy that is reflected from a target is the relative geometry between the source, receiver, and the target; a representation relevant to our simulation is given in Fig. 5.

To determine the impact that imperfect knowledge of the true target burial state has on performance we design an optimal transmit waveform using (7) based on the assumption that the target $G(\omega)$ is in the free-field. We then compute the theoretical performance based on (5) and (6) using each of the six true target responses represented by Figs. 2, 3, and 4. Subsequently, performance is analyzed in detail for two main cases (Examples 1 and 2). Both cases are similar in that they assume a flat noise power spectrum (PSD) $P_n(f) = 17$, a flat channel PSD $P_h(f) = 1$, and a transmit signal energy (E) scaled to achieve a signal-to-interference-noise-ratio of $SINR = -10dB$, where we define SINR by

$$SINR = 10\log_{10}\left(\frac{E}{\int P_n(\omega) + P_h(\omega) d\omega}\right) \tag{8}$$

We then consider the impact of colored interference, for which case we have previously shown increased benefits of optimal

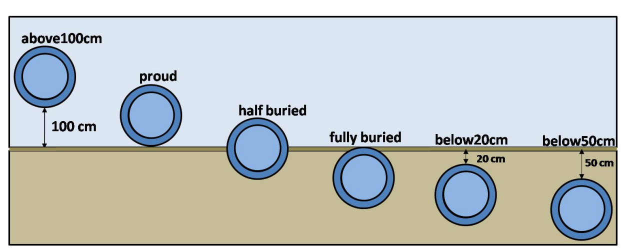

Fig. 2. Target burial states

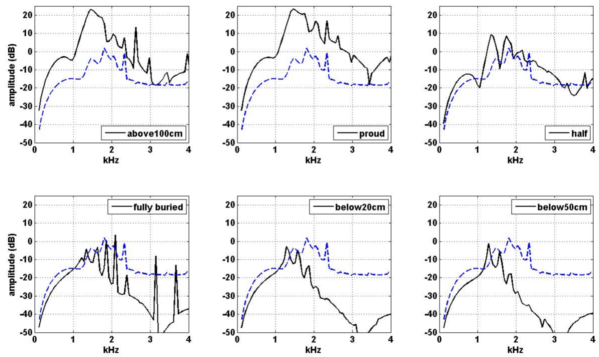

Fig. 3. Frequency domain responses of spherical shell in each of the six burial states over a 4kHz range. The solid line in each figure pane is the true target response in the indicated burial state while the dashed line is the same in each pane and represents the free-field response $G(\omega)$, used to design the "optimal" transmit spectrum.

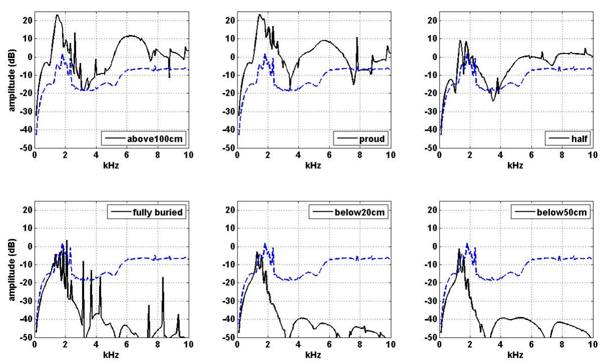

Fig. 4. Frequency domain responses of spherical shell in each of the six burial states over a 10kHz range. The solid line in each figure pane is the true target response in the indicated burial state while the dashed line is the same in each pane and represents the free-field response $G(\omega)$, used to design the "optimal" transmit spectrum.

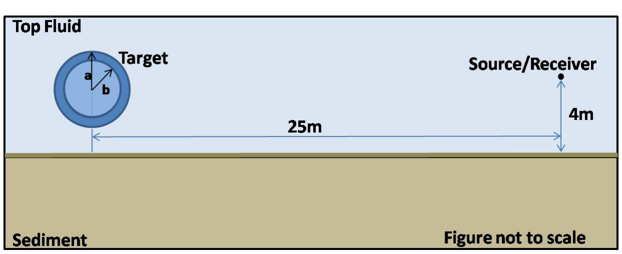

Fig. 5. Relative geometry between the source, receiver, and target

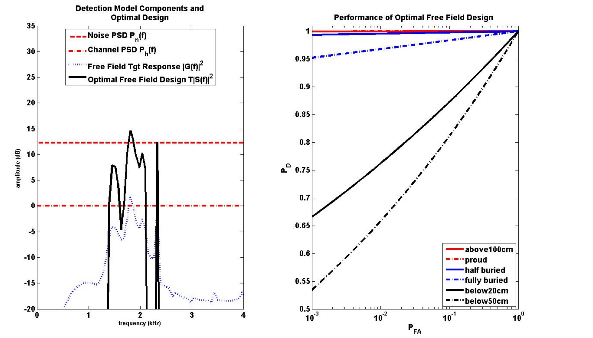

Fig. 6. LEFT: Model components and the optimal free-field design. RIGHT: ROC curves for each burial state

waveform design relative to the flat interference spectrum [6].

For comparison, detection performance is also obtained for a linear frequency modulated (LFM) transmit waveform with flat spectral magnitude, and two different bandwidths. As a point of clarification, for our purposes we refer to bandwidth as the range from $0Hz$ to the maximum frequency under consideration but we design signals and compute energies on the associated two-sided frequency range (i.e. $-f_{max}$ to f_{max}).

A. *Flat Interference Noise Spectrum*

1) Example 1, Design Bandwidth $4kHz$: In this section we consider the performance of the optimal design based on the free-field target response (up to $4\,kHz$), and an LFM waveform limited to $4\,kHz$. Figs. 6 and 7 show the performance associated with the optimal free-field waveform and the LFM waveform, respectively, in terms of ROC curves that plot the probability of detection (P_D) against the probability of false alarm (P_{FA}) on a log scale. Fig. 8 is a direct comparison of the ROC curves associated with the optimal free-field design and the $4kHz$ LFM waveform. These figures indicate that for both the optimal and LFM waveform, performance drops off considerably as the target becomes buried under sediment. The reason for the performance degradation can be understood by referring back to Fig. 3 and observing that as burial depth increases, the strength and location of the target resonances change relative to the free-field response. The consequence is that energy that was focused on frequencies relevant to the free-field target yield reduced backscattered power since those frequencies can become less pronounced when the target interacts with the sediment. This negative effect does not occur with the LFM waveform, since it has a flat spectrum over the frequency band of interest, and hence a shift in resonance has less impact on the effective backscatter power, relative to the optimal waveform. As a result, the LFM pulse can outperform the "optimal" waveform as the mismatch between the free-field target response (for which the optimal pulse was derived) and the true target response becomes greater, which is the case with increasing state of burial.

2) Example 2 Design Bandwidth: $10kHz$: Next we increase the design and transmit bandwidth to $10\,kHz$. The

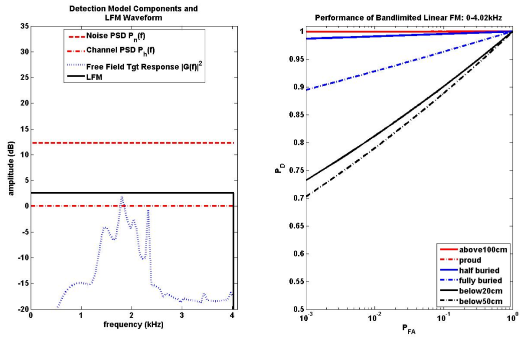

Fig. 7. LEFT: Model components and spectrum of 4kHz LFM waveform. RIGHT: ROC curves for each burial state

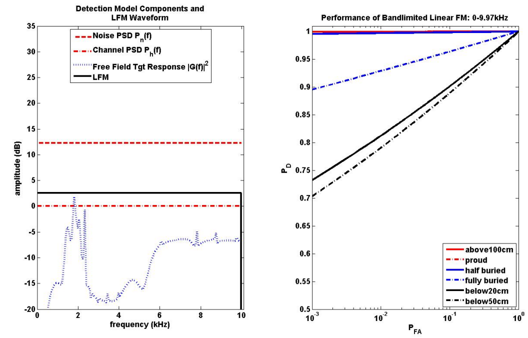

Fig. 10. LEFT: Model components and spectrum of 4kHz LFM waveform. RIGHT: ROC curves for each burial state

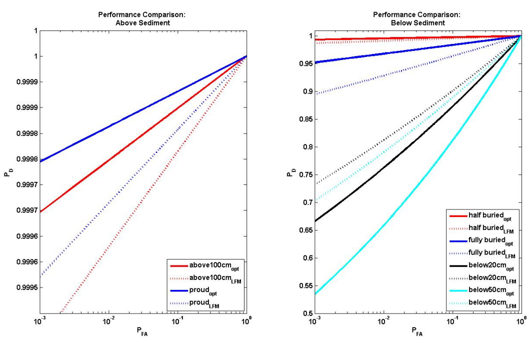

Fig. 8. LEFT: Above sediment ROC curves for optimal free-field and LFM waveforms. RIGHT: Below sediment ROC curves for optimal free-field and LFM waveforms

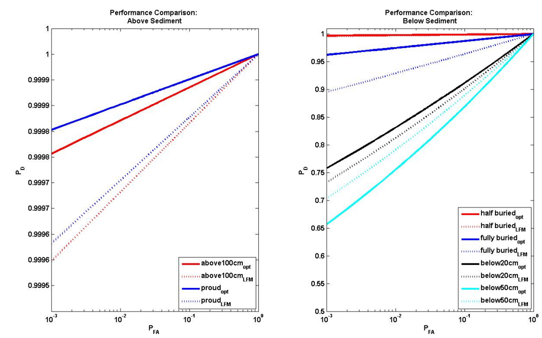

Fig. 11. LEFT: Above sediment ROC curves for optimal free-field and LFM waveforms. RIGHT: Below sediment ROC curves for optimal free-field and LFM waveforms.

relative performance between the optimal free-field design and the LFM waveform is essentially the same as in Example 1. It is noteworthy, however, to observe that the optimal free-field design shown in the left pane of Fig. 9 possesses frequency content that is somewhat more spread out over frequency, owing to the wider operating bandwidth. As a consequence, the performance gap between the optimal design and the LFM pulse is somewhat narrower than the $4\,kHz$ design presented previously, for the situations where the LFM outperforms the optimal waveform.

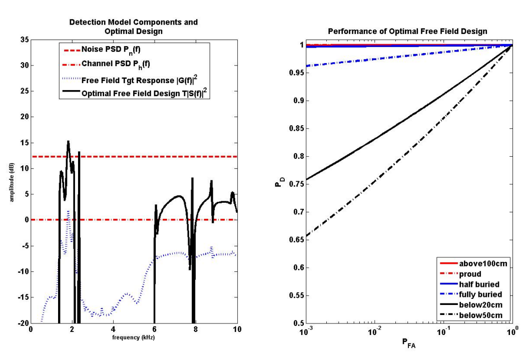

Fig. 9. LEFT: Model components and the optimal free-field design. RIGHT: ROC curves for each burial state

B. Colored Interference Noise Spectrum

1) Examples 3 and 4, Design Bandwidth $4kHz$ and $10kHz$: Figs. 14 and 17 show the performance comparisons for the colored noise case based on the $4kHz$ and $10kHz$ design bandwidths, respectively. There are two main observations that we can make from these figures. First, by comparing Figs. 14 and 17 to Figs. 8 and 11 we see that overall performance of both the optimal and LFM waveforms improves. The reason for this improvement is that the target has its most dominant resonances at low frequencies, and in the colored noise case there is relatively less noise power at these frequencies since the interference grows linearly with frequency. In other words, there is less interference noise power in the frequency range where there target responds the strongest, thereby yielding better overall performance in all cases. Second, we observe that the overall trend in performance between the optimal free-field design and the LFM waveform remains essentially as observed previously. That is to say that when the target is buried in the sediment the LFM out performs the optimal free-field design, while the optimal design somewhat outperforms the LFM waveform for non-buried targets.

Finally, an overall comparative summary of performance is given in Fig. 18. Each entry of the table corresponds to the area under the ROC curve associated with the particular scenario. The area under the ROC gives a gross characterization of overall performance, with 1 corresponding to perfect detection

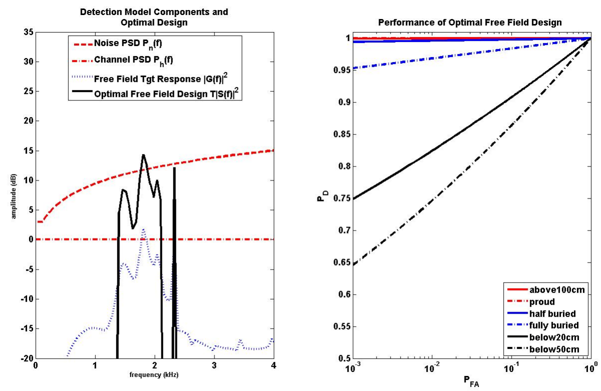

Fig. 12. LEFT: Model components and the optimal free-field design in colored noise. RIGHT: ROC curves for each burial state

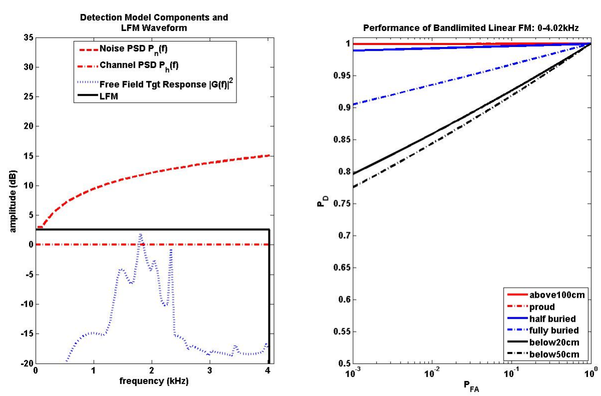

Fig. 13. LEFT: Model components and spectrum of 4kHz LFM waveform in colored noise. RIGHT: ROC curves for each burial state.

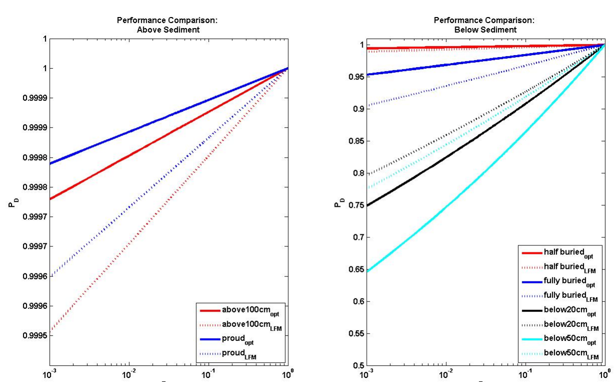

Fig. 14. LEFT: Above sediment ROC curves for optimal free-field and LFM waveforms in colored noise. RIGHT: Below sediment ROC curves for optimal free-field and LFM waveforms in colored noise

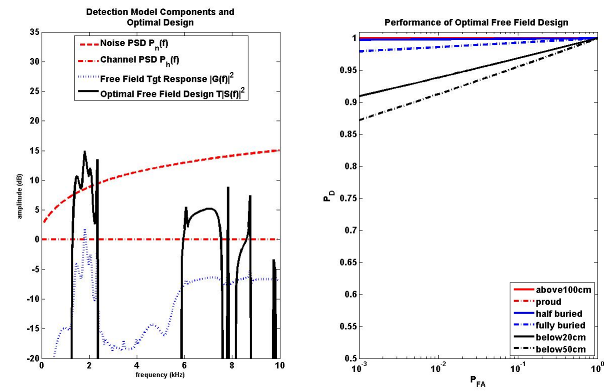

Fig. 15. LEFT: Model components and the optimal free-field design in colored noise. RGHT: ROC curves for each burial state.

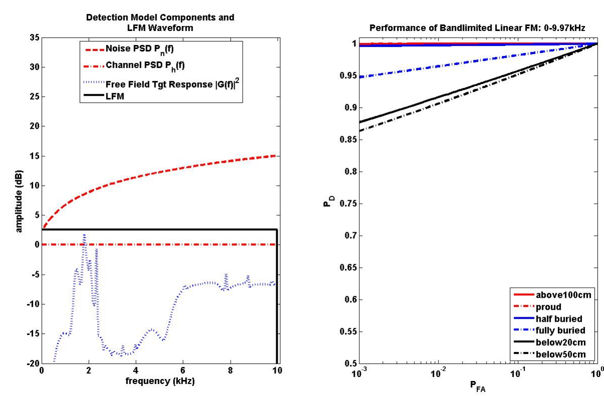

Fig. 16. LEFT: Model components and spectrum of 4kHz LFM waveform in colored noise. RIGHT: ROC curves for each burial state.

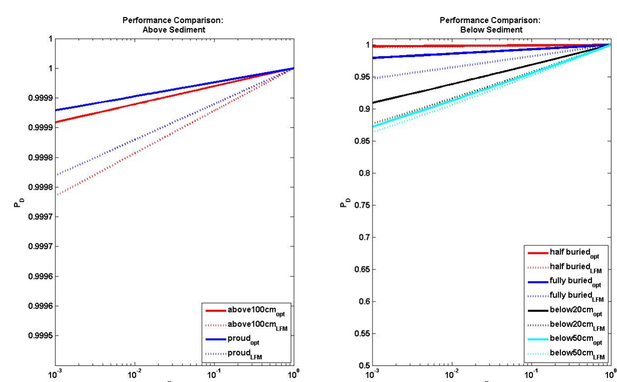

Fig. 17. LEFT: Above sediment ROC curves for optimal free-field and LFM waveforms in colored noise. RIGHT: Below sediment ROC curves for optimal free-field and LFM waveforms in colored noise.

		Flat Noise Spectrum		Colored Noise Spectrum	
		Optimal	LFM	Optimal	LFM
4kHz	above100cm	0.99996	0.99992	0.99999	0.99997
	proud	0.99997	0.99994	0.99999	0.99997
	half buried	0.99907	0.9981	0.99968	0.99703
	fully buried	0.99301	0.98417	0.99703	0.99231
	below20cm	0.94451	0.95691	0.98649	0.98143
	below50cm	0.91708	0.95152	0.98065	0.9792
		Optimal	LFM	Optimal	LFM
10kHz	above100cm	0.99998	0.99994	0.99999	0.99997
	proud	0.99998	0.99995	0.99999	0.99997
	half buried	0.99957	0.9994	0.99968	0.995
	fully buried	0.9945	0.98429	0.99703	0.99231
	below20cm	0.96151	0.95698	0.98649	0.98143
	below50cm	0.94371	0.95168	0.98065	0.9792

Fig. 18. Summary of detection performance, as measured by area under ROC

with no false alarms, and 0.5 corresponding to guessing.

IV. Conclusion

We have previously shown that optimal waveform design affords increasingly improved detection performance the more challenging the environment, relative to transmitting an LFM pulse [6]. Of course, such an approach requires knowledge of the channel interference and noise as well as the target frequency response. In this work, we examined via simulations the impact on detection performance of a mismatch between the expected target frequency response, for which the optimal waveform was designed, and the actual target frequency response which has been altered by the environment, such as occurs with buried objects. Six different target states were considered, ranging from within the water column, to proud, to completely buried, and for each case, detection performance was obtained using the optimal waveform designed to match the free-field target frequency response. Comparison of the (mismatched) "optimal" waveform was made to that of an LFM pulse over the same bandwidth as that used to design the optimal waveform. In general, for targets above the sediment layer, the optimal design afforded some performance gain over the LFM pulse, even though the target response did not match the free-field response for which the optimal pulse was designed. However, as the target became increasingly buried, such that the target frequency response became increasingly different from the free-field response, this gain was lost, and in fact the LFM pulse outperformed the "optimal" design for targets that were completely buried.

These results demonstrate that optimal waveform design can yield (modest) performance gains relative to an LFM pulse even when there is a mismatch between the expected frequency response and the actual frequency response of the target, to a degree. However, performance degrades significantly for buried objects, for both an LFM pulse and the "optimal" design based on the free-field response, and indeed the LFM pulse can outperform the (mismatched) optimal design in these cases. These results suggest that, for the detection of buried objects, it is important to incorporate knowledge of the burial state into the optimal design. Alternately, another approach could be to design an optimal waveform that maximizes the minimum P_D over a family of target responses $G(\omega)$ – such as those in Fig. 2,3. We are currently investigating these and related issues.

V. Acknowledgment

This research was supported by a grant from the Office of Naval Research (N00014-09-1-0448).

References

[1] P. M. Woodward, Probability and Information Theory, with Applications to Radar, McGraw-Hill Book Co., Inc., 1953.

[2] M. Bell, " Information theory and radar waveform design," IEEE Trans. Inf. Theory, vol. 39, no. 5, pp. 1578-1597, Sept. 1993.

[3] Y. Yang R. Blum, "MIMO radar waveform design based on mutual information and minimum mean-squared error estimation," *IEEE Trans. Aerospace and Electronic Systems*, vol. 43, no. 1, pp. 330-343, Jan. 2007

[4] S. Kay, "Optimal signal design for detection of gaussian point targets in stationary gaussian clutter/reverberation," *IEEE J. Sel. Topics in Sig. Proces. Mag.*, vol. 1, no. 1, pp. 31-41, Jun. 2007.

[5] S. Kay, "Waveform design for multistatic radar detection," *IEEE Trans. Aerospace and Electronic Systems*, vol. 45, no. 3, pp 1153-1166, Jul. 2009

[6] B. Hamschin and P. Loughlin, "Optimal time and frequency domain waveform design for target detection," *Proc. SPIE, Automatic Target Recognition XX*, Defense, Sensing and Security Symposium, vol. 7696, Apr. 2010.

[7] J. Li, J. R. Guerci, and L. Xu, "Signal waveform's optimal-under-restriction design for active sensing," *IEEE Signal Processing Letters*, vol. 13, no. 9, Sept. 2006.

[8] A. Papandreou-Suppappola, A. Nehorai, and R. Calderbank (Eds.), "Waveform agility in radar systems [Special Issue]," *IEEE Signal Processing Magazine*, vol. 26, no. 1, Jan. 2009.

[9] J. J. Zhang, A. Papandreou-Suppappola, B. Gottin, and C. Ioana, "Time-frequency characterization and receiver waveform design for shallow water environments,"*IEEE Trans. on Signal Processing*, vol. 57, no. 8, Aug. 2009.

[10] S. U. Pillai, H. S. Oh, D. C. Youla, and J. R. Guerci, "Optimal transmit-receiver design in the presence of signal-dependent interference and channel noise," *IEEE Trans. Inf. Theory*, vol. 46, no. 2, pp. 577-584, Mar. 2000.

[11] L. Cohen, Time-Frequency Analysis, Prentice-Hall, 1995.

[12] H. Stark and Y. Yang, Vector Space Projections - A Numerical Approach to Signal and Image Processing, Neural Nets, and Optics, John Wiley & Sons, Inc., 1998.

[13] R. Lim, "Multiple scattering by many bounded obstacles in a multilayerd acoustic medium," *J. Acoust. Soc. Am.*, vol. 92, no. 3, pp. 1593-1612, 1992.

[14] R. Lim, J. L. Lopes, R. H. Hackman, and D. G. Todroff, "Scattering by objects in underwater sediments: theory and experiment," *J. Acoust. Soc. Am.*, vol. 93, no. 4, pp. 1762-1783, 1993.

[15] R. Lim, "Scattering by an obstacle in a plane stratified poroelastic medium: application to an obstacle in ocean sediments," *J. Acoust. Soc. Am.*, vol. 95, no. 3, pp. 1223-1244, 1994.

[16] R. Lim, "Acoustic scattering by a partially three-dimensional elastic obstacle," *J. Acoust. Soc. Am.*, vol. 104, no. 2, pp. 769-782, 1998.

[17] R. Lim, "Measurements and modeling of acoustic scattering from partially and completely buried spherical shells," *J. Acoust. Soc. Am.*, vol. 112, no. 5, pp. 1817-1830, 2002.